Article:
Jackson, V, Hermann, J, Tynan, CJ et al. (11 more authors) (2022) The guidance and adhesion protein FLRT2 dimerizes in cis via dual small-X3-small transmembrane motifs. Structure, 30 (9). pp. 1354-1365. ISSN 0969-2126

https://doi.org/10.1016/j.str.2022.05.014

Supplementary Material for

The guidance and adhesion protein FLRT2 dimerizes *in cis* via dual Small-X_3-Small transmembrane motifs

Verity Jackson[#,1], Julia Hermann[#,1,6], Christopher J. Tynan[#,2], Daniel J. Rolfe[2], Robin A. Corey[1], Anna L. Duncan[1], Maxime Noriega[3], Amy Chu[1], Antreas C. Kalli[4], E. Yvonne Jones[5], Mark S. P. Sansom[1], Marisa L. Martin-Fernandez[*,2], Elena Seiradake*[*,1], Matthieu Chavent*[*,3,7]*

#These authors contributed equally to this study

1- Department of Biochemistry, University of Oxford, South Parks Road, Oxford, OX1 5RJ, United Kingdom
2- Central Laser Facility, Research Complex at Harwell Science & Technology Facilities Council, Harwell Campus, Didcot, United Kingdom
3- Institut de Pharmacologie et Biologie Structurale, IPBS, Université de Toulouse, CNRS, UPS, 205 route de Narbonne, 31400, Toulouse, France
4- Department of Discovery and Translational Science, Institute of Cardiovascular and Metabolic Medicine, School of Medicine and Astbury Center for Structural Molecular Biology, University of Leeds, United Kingdom
5- Division of Structural Biology, Wellcome Centre for Human Genetics, University of Oxford, Oxford, United Kingdom
6- Present address: German Cancer Research Center (DKFZ), Im Neuenheimer Feld 581, 69120 Heidelberg, Germany
7- Lead contact

Corresponding authors: Elena Seiradake (email: elena.seiradake@bioch.ox.ac.uk), Marissa L. Martin-Fernandez (email: marisa.martin-fernandez@stfc.ac.uk), Matthieu Chavent (email: matthieu.chavent@ipbs.fr)

This PDF file includes 6 figures with legend.

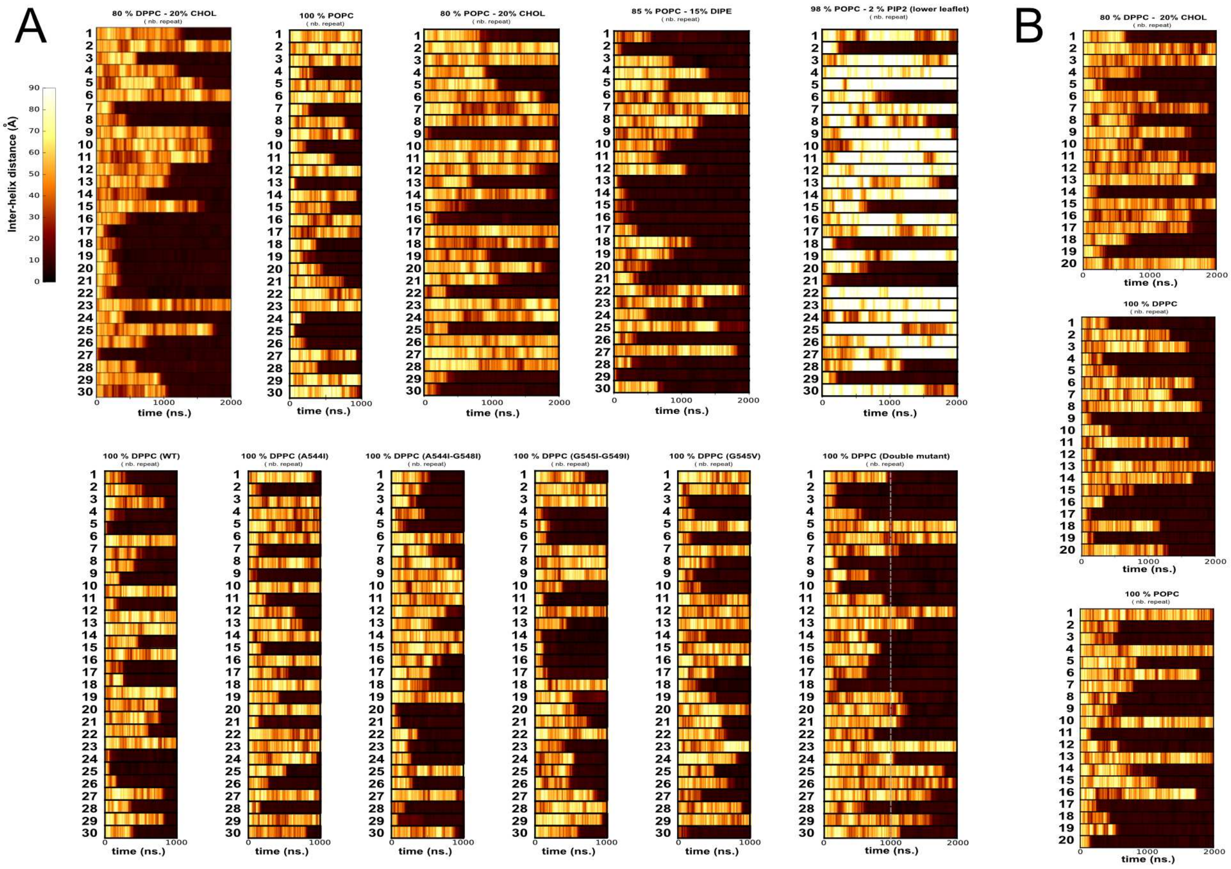

Figure S1: Distance between the TM_{32} and TM_{24} monomers in different type of membranes, related to figure 1. A- Distance between the two TM_{32} helices as a function of the time during the course of the CG-MD simulation for the WT and mutants (double mutant corresponds to A544I-G548I+G545I-G549I, see Fig. 5A for the mutations details). The two helices are first positioned 60 Å apart and then freely diffuse in the membrane. For the double mutant, too few simulations depicted interacting domains after 1 µs to perform meaningful analysis, so these simulations were extended to 2 µs. For the POPC-PIP2 composition, we constructed larger system to have a minimal number of PIP_2 lipids hence possibly increasing the potential distance between TM. **B-** Distance between the two TM_{24} helices as a function of time during the course of the CG-MD simulation for 3 different membrane compositions: 80% DPPC + 20% cholesterol, 100% DPPC, and 100% POPC.

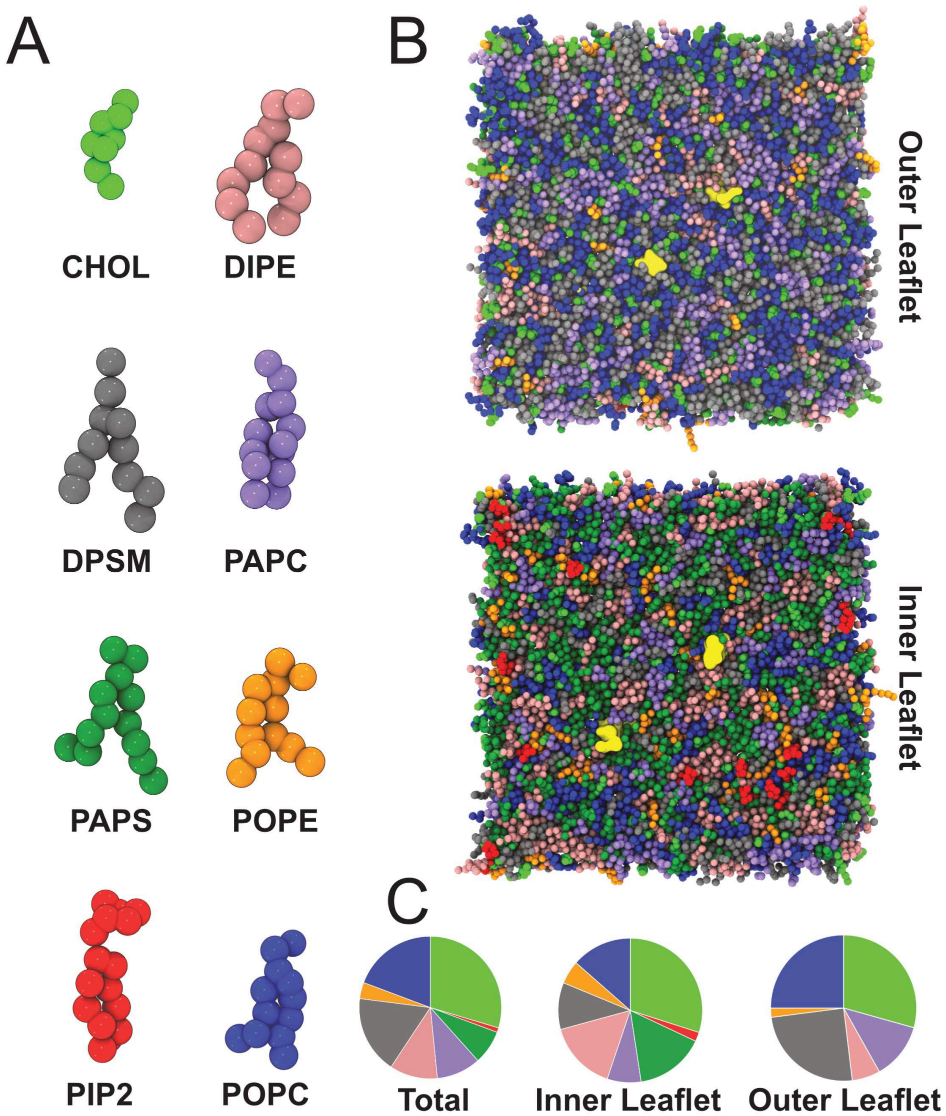

Figure S2: Plasma membrane composition, related to figure 2. A- Coarse-grained models of each lipid constituting the plasma membrane. **B-** Equilibrated model of the plasma membrane model with colors corresponding to colored lipids in A. In yellow the starting positions of the two TM_{32} domains. **C-** Lipid distributions for each leaflet and in total.

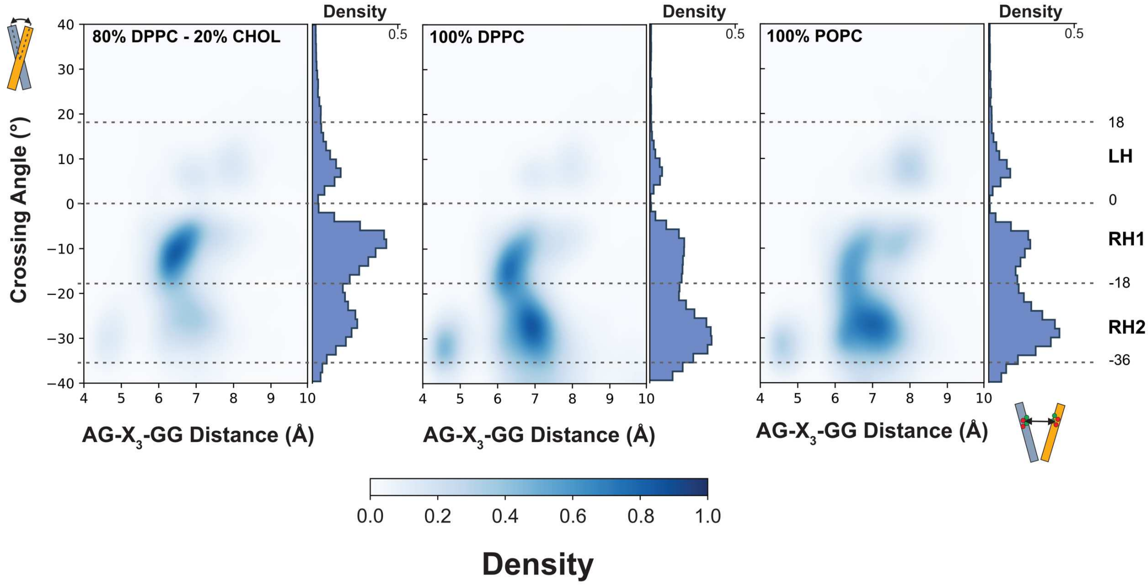

Figure S3: Helix crossing angle distributions for TM_{24} dimers, related to figure 3. Averaged helix crossing angle distribution for TM_{24} systems based on individual simulations for different membrane compositions in which TM domains interacted for at least two hundreds of nanoseconds.

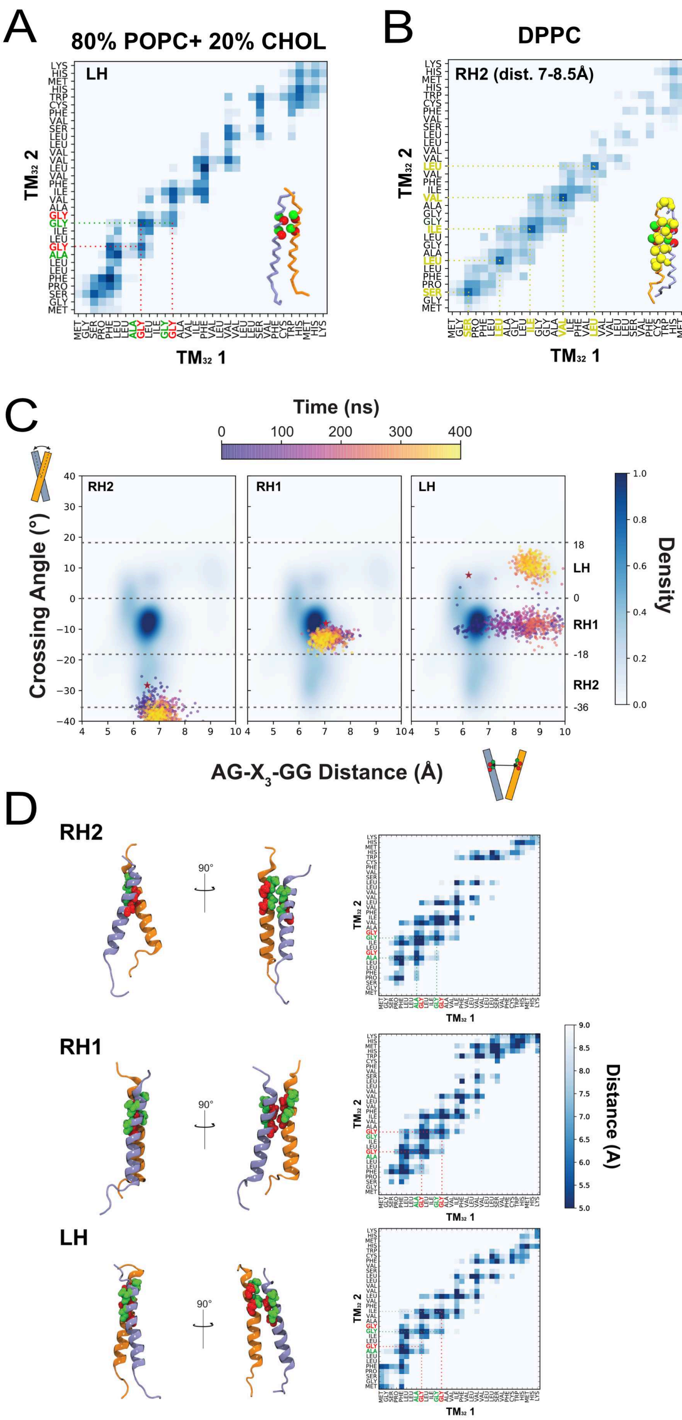

Figure S4: TM interactions in Coarse-grain and AT simulations, related to figure 4. A- Averaged TM contact matrix extracted from simulations of TM_{32} in 80% DPPC + 20% of cholesterol for the LH population displaying a TM interaction involving both G_{544}-X_3-G_{548} (green) and G_{545}-X_3-G_{549} (red) motifs. **B-** Occasionally, neither G_{544}-X_3-G_{548} (green) or G_{545}-X_3-G_{549} (red) motifs were present at the interface as seen for one RH2 population extracted from DPPC simulations. **C-** We converted in atomistic representation the three main representative structures of the dimer embedded in a 80% DPPC + 20% cholesterol membrane. We converted TM dimer structures used in the DPPC+CHOL membrane because the atomistic models of the lipids constituting the PM membrane were, to our knowledge, not all parametrized for atomistic force fields. Furthermore, compared to DPPC and POPC membranes, the TM dimer populations in the DPPC+CHOL membrane are the most similar to those in the PM membrane (Fig. 3). For each representative conformation, crossing angles populations based on atomistic simulations are colored in function of the time. These crossing angles are superimposed to the averaged population obtained from CG simulations. The starting structure is represented by a red star. **D-** In each case, a contact map calculated during the course of the 400 ns simulation and a final structure of the helix dimer are shown.

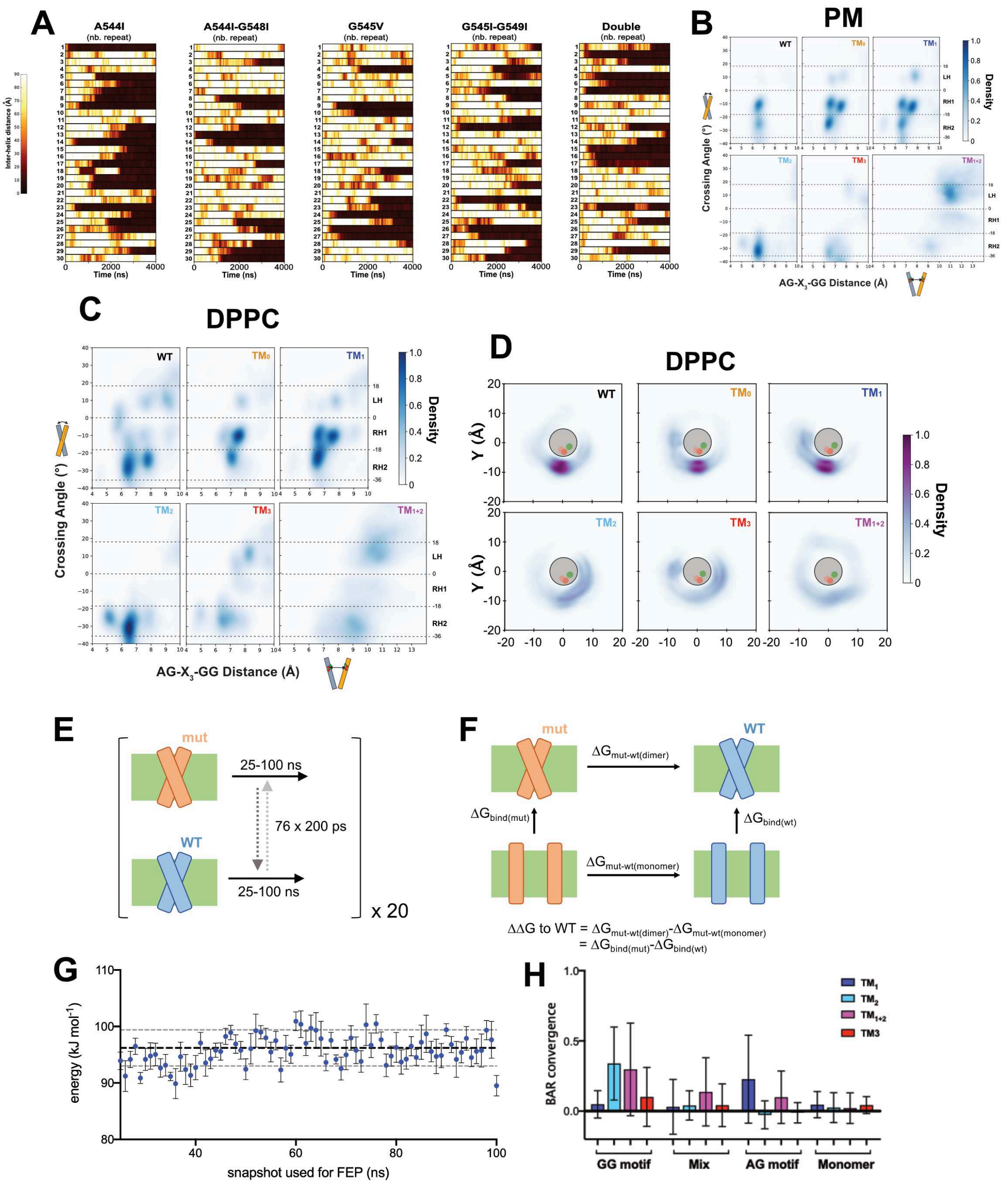

Figure S5: Effects of mutations, related to figure 5. A- Distance between the two TM_{32} helices as a function of the time during the course of the CG-MD simulation for the mutants in the PM. The two helices are first positioned 60 Å apart and then freely diffuse in the membrane. **B-** TM_{32} WT and mutants structural populations in the PM bilayer. **C-** TM_{32} WT and mutants structural populations in a DPPC bilayer. **D-** Spatial distribution profiles of one TM_{32} helix relative to the other for the CG simulations of both WT and mutants in a DPPC bilayer. **E-** Overview of non-equilibrium FEP scheme. For each dimer/monomer system, 100ns simulations are run in state 0 ('mut') or state 1 ('WT'). Snapshots are taken every 1 ns from 25-100 ns, and subjected to 200 ps FEP from either state 0 to 1 or vice versa. This process is repeated 20 times for statistics. **F-** Thermodynamic cycle for calculating $\Delta\Delta G$ values. The top and bottom lateral ΔG values are explicitly calculated here in the non-equilibrium FEP, allowing calculation of a $\Delta\Delta G$ using the equation. **G-** Example plot showing how the ΔGmut-WT(dimer) values change depending on input snapshot. A regular spread of data across the data suggests that the dimers are stable and are not shifting in conformation during the equilibrium simulation. Shown are the data for the RH2 TM1+2 mutant, which gives one of the higher $\Delta\Delta G$ values so would be expected to change the most. **H-** Convergence analysis measuring the degree of overlap between the forward and reverse FEP calculations, based on (Hahn and Then, 2010) and implemented in pmx (Gapsys et al., 2015). Here, a value of less than ca. 0.8 is considered as having sufficient overlap to show convergence.

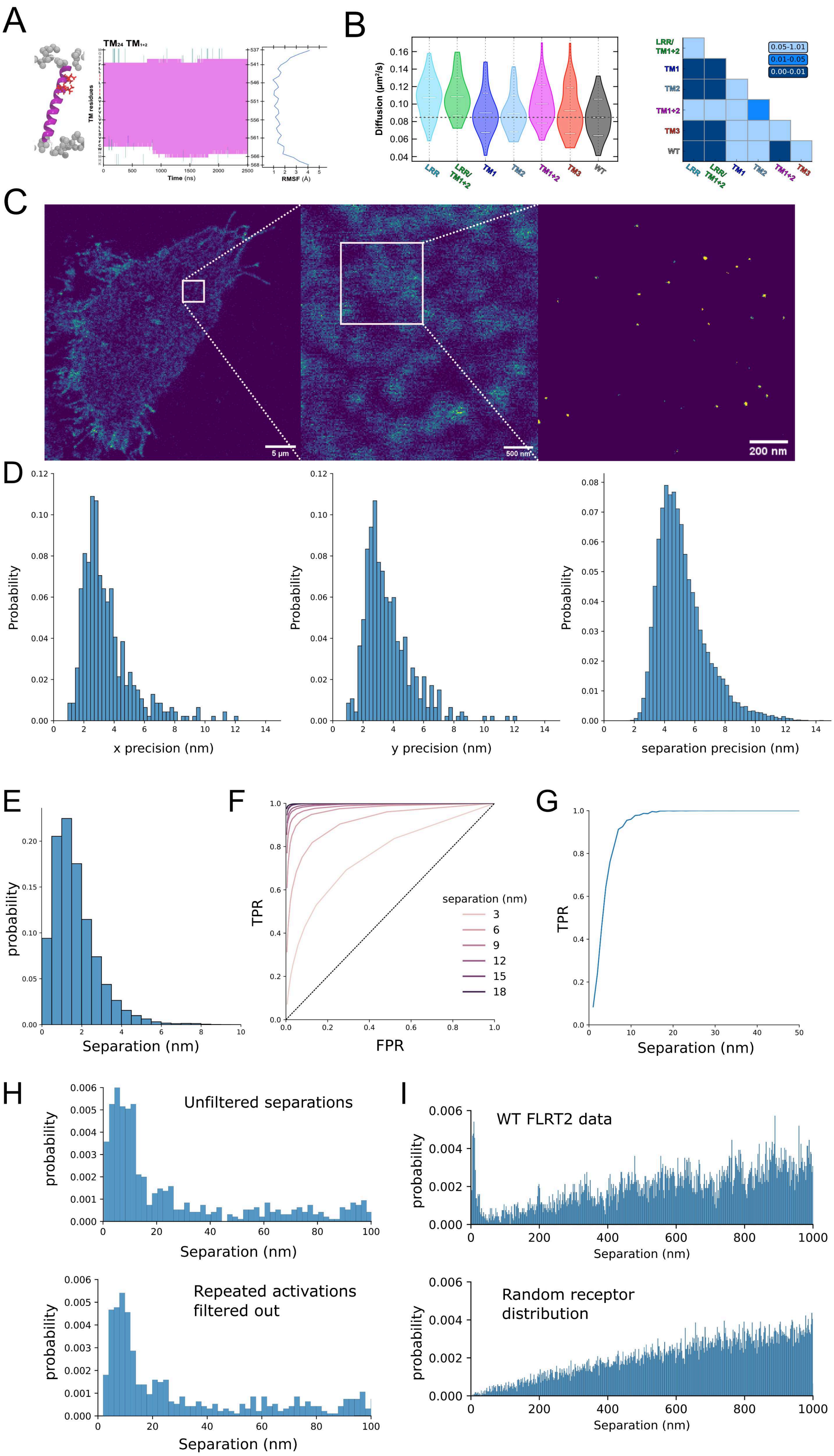
A
B
C
D
E
F
G
H
I
Diffusion (µm²/s)
LRR
LRR/TM1+2
TM1
TM2
TM1+2
TM3
WT
0.05-1.01
0.01-0.05
0.00-0.01
5 µm
500 nm
200 nm
Probability
x precision (nm)
y precision (nm)
separation precision (nm)
probability
Separation (nm)
TPR
FPR
separation (nm)
Unfiltered separations
Repeated activations filtered out
WT FLRT2 data
Random receptor distribution

Fig. S6: Atomistic simulation and MinFlux analysis, related to Figure 6. A- Atomistic simulation of the TM_{1+2} mutant in a POPC bilayer showing an overall stable secondary structure during the course of the simulation. **B-** Left: distribution of instantaneous diffusion coefficient (D) for wtFLRT2 and each of the six FLRT2 mutants tested. Right: Significance analysis of the distributions presented in A based on a Kolmogorov-Smirnov test (more details in Methods section). **C-** From left to right: A confocal image of the bottom membrane of HeLa cells expressing wtFLRT2-SNAP labelled with SNAP Surface Alexa 647. A 4 µm x 4 µm region of interest is selected for MINFLUX imaging. A section of the MINFLUX reconstruction of this region shows that resolved into discrete fluorescence emitters. The reconstructed MINFLUX image is a histogram of localisations with a bin size of 4nm chosen for presentation clarity. **D-** From left to right: Distributions of x-precision, y-precision and the precisions of measured separations between emitters aggregated from the wtFLRT2 MINFLUX datasets. **E-** Simulated pairs of localisation bursts with zero separation randomly generated using the x, y-precisions and burst sizes of the real wtFLRT2 datasets demonstrate that any repeated activations of the same emitter during a MINFLUX measurement will produce measurable short separations. **F-** The performance of the Hotelling's t-squared test on simulated data to correctly classify pairs of localisation bursts as derived from the same or from different emitters. The false negative rate (FNR) is the proportion of pairs incorrectly identified as not being at the same emitter location. The true positive rate (TPR) is the proportion of pairs correctly identified as being from different emitter locations. The dotted line indicates where a classifier performs no better than random selection. As the p-value threshold is reduced, the FPR approaches zero. However, as the separation of the true approaches zero so does the TPR. **G-** A p-value threshold of 0.01 predicts a FPR of 0.028, where 2.8% of pairs derived from repeated activations of the same emitter will be incorrectly included in the distribution of separations. **H-** The distribution of separations obtained from the wtFLRT2 2D MINFLUX datasets before and after removal of repeated activations using the Hotelling's t-squared test and a p-value threshold of 0.01. **I-** The distribution of separations obtained from wtFLRT2 and the peak at ~10nm is inconsistent with the distribution of separations expected from randomly distributed receptors.